The retinitis pigmentosa 28 protein FAM161A is a novel ciliary protein involved in intermolecular protein interaction and microtubule association

Frank Zach[1], Felix Grassmann[1], Thomas Langmann[1,2], Nasrin Sorusch[3], Uwe Wolfrum[3] and Heidi Stöhr[1,*]

[1]Institute of Human Genetics, University of Regensburg, Regensburg, Germany, [2]Center of Ophthalmology, Department of Experimental Immunology of the Eye, University of Cologne, Cologne, Germany and [3]Institute of Zoology, Johannes Gutenberg University of Mainz, Mainz, Germany

Loss-of-function mutations in the gene encoding FAM161A were recently discovered as the cause for RP28, an autosomal recessive form of retinitis pigmentosa. To initiate the characterization of the cellular role of FAM161A in the retina, we focused on its subcellular localization and conducted *in vitro* studies to identify FAM161A-interacting proteins and associated cellular structures. Immunohistochemistry revealed the presence of mouse FAM161A in the photoreceptor inner segments, the synaptic regions of the outer and inner plexiform layers and the ganglion cells. In mouse and human retinal sections from unfixed eyes, FAM161A localized to the ciliary region linking photoreceptor outer and inner segments. High-resolution immunofluorescence and immunoelectron microscopy mapped FAM161A to the connecting cilium, the basal body region and the adjacent centriole. Ectopic FAM161A was found in the centrosome and concentrated at the base of primary cilia in cultured cells. In addition, overexpressed FAM161A was clearly associated with microtubules during interphase and mitosis. The presence of FAM161A increased microtubule acetylation and stabilization. We further show that the evolutionarily conserved UPF0564 domain of FAM161A is crucial for its binding to microtubules and mediates homo- and heterotypic FAM161A and FAM161B interaction. In conclusion, our study shows that FAM161A is a microtubule-associated ciliary protein presumably involved in microtubule stabilization to maintain the microtubule tracks and/or in transport processes along microtubules in photoreceptors and other retinal cell types.

INTRODUCTION

Retinitis pigmentosa [RP (MIM 268000)] is the most common form of inherited retinal disease with X-linked, autosomal dominant or autosomal recessive inheritance patterns. RP has an estimated prevalence of 1:4000 (1) and thus affects nearly one and a half million people worldwide. RP patients typically experience night blindness and progressive bilateral visual field restriction due to rod photoreceptor degeneration followed by a loss of cone function in advanced stages. Disease progression is highly variable but may ultimately lead to legal blindness. Remarkably, mutations in 45 different genes have so far been associated with non-syndromic RP

(Retinal Information Network, http://www.sph.uth.tmc.edu/Retnet/) affecting various functional and structural features of the retina and the retinal pigment epithelium. This includes components of the phototransduction cascade and the visual cycle, the regulation of retinal gene expression but also general cellular processes like splicing, protein modification and degradation. A growing number of RP genes encode proteins localized at the base of and within the connecting cilium as well as the outer segment axoneme of photoreceptor cells. Photoreceptor outer segments are initially formed from primary cilia in photoreceptor precursors and thus represent highly modified cilia which contain a microtubule-based axoneme projecting from basal bodies (2). Due to the high

*To whom correspondence should be addressed at: Institute of Human Genetics, University of Regensburg, Franz-Josef-Strauss-Allee 11, 93053 Regensburg, Germany. Tel: +49 9419445428; Fax: +49 9419445402; Email: heidi.stoehr@klinik.uni-regensburg.de

turnover of phototransductive disk membranes, photoreceptor outer segments require high and constant supply of proteins and lipids for their development and maintenance. These components are synthesized in the inner segments and need to be transferred across the connecting cilium to the site of disk assembly at the proximal end of the outer segments. Defects in ciliary components can cause not only isolated RP but also syndromic forms involving several organs in addition to the retina, such as Usher syndrome and Bardet–Biedl syndrome (BBS) (3).

We have recently identified a p.Arg229X stop mutation in exon 3 of the human *FAM161A* gene on chromosome 2p15 as the cause for RP28 (4), an autosomal recessive form of RP originally mapped to chromosome 2p11-p15 in a consanguineous Indian family (5). Concomitantly, additional stop and frameshift mutations in *FAM161A* were found in RP patients from Germany, Israel and the Palestinian territories (4,6) implicating that a loss of FAM161A leads to retinal degeneration in humans. The *FAM161A* gene is composed of at least seven exons that are alternatively spliced to produce two major isoforms of 660 amino acids (76 kDa) and 716 amino acids (83 kDa), respectively. Both variants have similar expression profiles with high transcript levels in the retina and testis. The mouse ortholog, *Fam161a*, is also highly expressed in the developing and adult retina and a direct target of the transcription factor CRX (4).

FAM161A belongs to an uncharacterized protein family which shares an evolutionarily conserved region in the C-terminal part, the so-called UPF0564 domain of unknown function. The UPF0564 domain consists of ∼400 amino acid residues and can be found in various eukaryotic species including vertebrates, insects, nematodes, protozoa and yeast as well as in bacteria. The human genome contains one paralog of the *FAM161A* gene, *FAM161B*, which is located on chromosome 14q24.3. FAM161A and FAM161B share 25% overall sequence identity on the protein level with an even higher level of sequence identity across the UPF0564 domain (35%). FAM161B was previously identified as a physical interactor of TACC3 (transforming acidic coiled-coil 3), an interaction that is conserved across species (7,8). TACC3 plays important roles in centrosome-dependent microtubule assembly, kinetochore attachment, chromosome alignment and the regulation of mitotic exit (8). FAM161A was detected in the cytoskeleton fraction of the mouse photoreceptor sensory cilium complex by a proteomic analysis (9). In a more recent proteomics approach using lymphoblastic KE37 cells, FAM161A was found to be a constituent of human centrosomes (10). Taken together, these studies suggest a possible function of FAM161 family members in microtubule-network organization and centrosome biology.

In the current study, we aimed to gain further insight into the function of FAM161A with specific emphasis on the cellular localization of this protein in mouse photoreceptors and the functional characterization of the conserved UPF0564 domain. We demonstrate the presence of FAM161A in the connecting cilium, the basal body and the adjacent centriole of photoreceptor cells and thus designate FAM161A as a novel ciliary protein. Consistent with this observation, ectopic FAM161A was found to be recruited to centrosomes and to be concentrated at the base of primary cilia in LLC-PK1

cells, a cultured cell line derived from porcine renal proximal tubule cells. Furthermore, FAM161A localized to and stabilized cytoplasmic microtubules and became associated with spindle and spindle pole microtubules during mitosis. Biochemical analyses revealed that the conserved UPF0564 domain mediates FAM161A microtubule association as well as homo- and heterodimerization of FAM161 proteins. Therefore, we hypothesize that FAM161A may be a scaffolding protein that is important for microtubule stabilization and/or microtubule-based transport processes along cytoplasmic and ciliary microtubules.

RESULTS

Subcellular localization of FAM161A in the retina

To investigate the subcellular localization of FAM161A in mouse retina, we generated a rabbit polyclonal antiserum (anti-mFAM161A) against the N-terminal portion of mouse FAM161A [glutathione-*S*-transferase (GST)-mFAM161A amino acids 14–355]. Following affinity purification, the specificity of the polyclonal anti-mFAM161A antibody was verified by specific reactivity to maltose binding protein (MBP)-mFAM161A amino acid 14–355 recombinant protein and overexpressed full-length FAM161A as well as by the lack of anti-mFAM161A immunoreactivity on mouse retinal sections using antibodies preadsorbed with excess MBP-mFAM161A amino acids 14–355 (Supplementary Material, Fig. S1A–C). In retinal sections from adult paraformaldehyde (PFA)-fixed mouse eyes, the affinity-purified anti-mFAM161A antibody strongly labeled the inner segments of photoreceptor cells and the outer plexiform layer (Supplementary Material, Fig. S1D), confirming the earlier reports of FAM161A localization using an anti-peptide antibody (4). The FAM161A protein was found to be located in the cytoplasm of the inner segments bounded by the distribution of the secretory RS1 protein along the surface membranes of the inner segments of rod and cone photoreceptors (Supplementary Material, Fig. S1E). FAM161A staining did neither overlap with rhodopsin (Rho) labeling in the outer segment membranes (data not shown) nor retinitis pigmentosa-1 (RP1) immunoreactivity along microtubules of the outer segment portion of the photoreceptor axoneme (11) (Supplementary Material, Fig. S1F), suggesting that FAM161A localization is restricted to the inner segments of mouse photoreceptors. In addition to the previously used anti-peptide antibody, anti-mFAM161A also stained the inner plexiform and the ganglion cell layer (Supplementary Material, Fig. S1D). Since pre-embedding fixation has previously been shown to interfere with certain antibody staining in the connecting cilia of photoreceptor cells (12,13), we next used cryosections of mouse eyes that were embedded without PFA fixation for immunohistochemistry. In unfixed mouse retinal sections, FAM161A immunoreactivity was detected in elongated structures in the narrow region between the outer and inner segments of the photoreceptor layer that most likely correspond to the connecting cilia (Fig. 1A and B). Using a commercial antibody toward human FAM161A, predominant staining of the structural link between outer and inner segments was also observed in human photoreceptors (Fig. 1C). FAM161A immunoreactivity
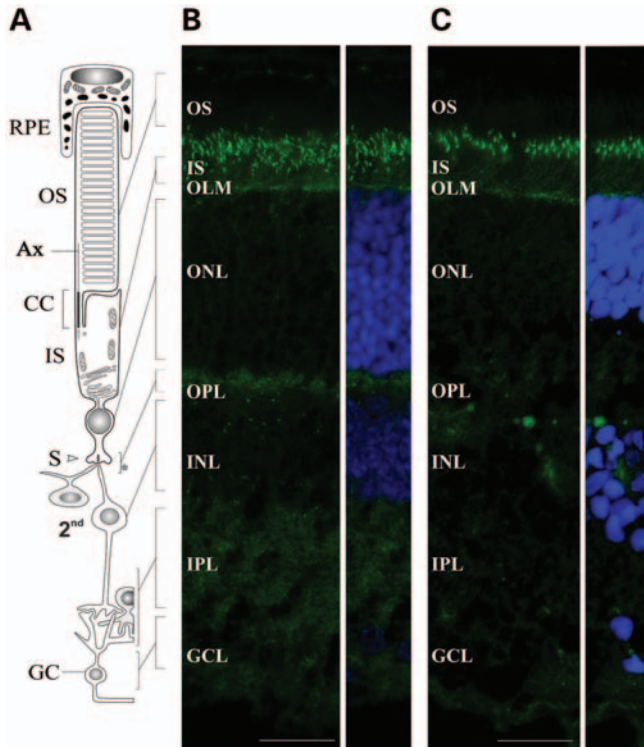
Figure 1. Localization of FAM161A in the retina. (**A**) Scheme of retinal layers. Indirect immunofluorescence analyses of FAM161A localization (green) in retinal cryosections generated from unfixed (**B**) mouse and (**C**) human eyes. Scale bars, 25 μm. Counterstaining with 4',6-diamidino-2-pheny-lindole (DAPI) (blue) reveals the different layers of the retina as shown in the merged images on the right. OS, outer segment; IS, inner segment; OLM, outer limiting membrane; ONL, outer nuclear layer; OPL, outer plexiform layer; INL, inner nuclear layer; IPL, inner plexiform layer; GCL, ganglion cell layer. Immunostaining of mouse retina was performed with antibodies toward mFAM161A, labeling of human retina with antibodies toward hFAM161A. Strong FAM161A immunoreactivity in the junctional region between outer and inner segments can be observed in sections from both mouse and human eyes.

in the inner segments and the inner retinal layers was generally fainter in unfixed when compared with PFA-fixed tissue.

Double-labeling experiments were then performed to further define the subcellular localization of FAM161A by comparing the FAM161A immunoreactivity with markers for different regions of mouse photoreceptors (Fig. 2). FAM161A staining was found proximal to RP1 immunoreactivity in the outer segment portion of the photoreceptor axoneme, a subciliary region that comprises the connecting cilium, the basal body and the adjacent centriole (Fig. 2A and A′). Consistent with a distribution of FAM161A in these subciliary compartments, FAM161A completely co-localized with centrin 3, a marker for the connecting cilium, basal body and adjacent centriole (14) (Fig. 2B and B′). In the connecting cilium region, FAM161A immunoreactivity also overlapped with that for acetylated α-tubulin, a marker of stabilized microtubules in the ciliary axoneme (Fig. 2C, C′ and D). A short region of axo-nemal microtubules at the outer segment base extending from the connecting cilium, however, was only labeled by anti-acetylated α-tubulin antibodies (Fig. 2C and C′) and likely overlaps with the small gap between RP1 and FAM161A staining (Fig. 2A and A′). When compared with

the anti-acetylated α-tubulin immunofluorescence, FAM161A labeling was brighter at the proximal end of the connecting cilium, indicating the abundance of FAM161A at the basal body complexes which serve as microtubule organizing centers in photoreceptors (15).

We also aimed to more precisely assess the localization of FAM161A in the outer plexiform layer and co-stained mouse retinal sections with antibodies toward RIBEYE, a marker for the photoreceptor ribbon synapse (16), and FAM161A. The double-labeling experiment revealed no clear overlap between the RIBEYE-immunoreactive ribbon synapses and FAM161A-positive punctuate structures (Fig. 2E and E′), indicating that FAM161A is present in postsynaptic terminals of second-order neurons (Fig. 2F).

Ultrastructural localization of FAM161A in the ciliary region

High-resolution analysis by immunoelectron microscopy was used to determine the ultrastructural localization of FAM161A. Our data from electron microscopy confirmed the subciliary distribution of FAM161A to the microtubules of the connecting cilium, the basal body and the adjacent centriole (Fig. 3A–D). Note that the central region of the connecting cilium is not labeled since antibodies do not reach the epitopes in connecting cilia in pre-embedding labeling protocols (17–19). FAM161A labeling was specifically found at the microtubule doublets but not in the subciliary compartments of the lumen or associated with the membrane of the connecting cilium (Fig. 3A–C). Substantial labeling of FAM161A was found in the basal body and at the adjacent centriole (Fig. 3A and D). FAM161A was mostly absent from the distal axoneme of the outer segment, the outer segment itself and the periciliary extension of the apical inner segment (Fig. 3A). Only sparse anti-FAM161A labeling was found in the inner segment. Furthermore, in the other non-ciliated retinal cells, we detected FAM161A in the centrosomes, present both at centrioles and in centriolar satellites of the pericentriolar matrix (Fig. 3E).

Subcellular localization of recombinant FAM161A in mammalian cells

We next examined the subcellular localization of recombinant FAM161A in mammalian cells. Immunofluorescence micros-copy of COS-7 cells overexpressing the short isoform of FAM161A with a C-terminal Rho1D4 tag revealed that during interphase FAM161A-1D4 localized to a fiber-like structure in the cytoplasm that completely overlapped with the microtubule labeling produced by anti-α-tubulin antibodies (Fig. 4A). The pattern of the microtubule network in cells expressing high levels of FAM161A slightly changed to a more circular morph-ology with increased α-tubulin staining indicating bundled microtubules. The unusually thick microtubule network induced by FAM161A overexpression was heavily acetylated as shown by immunostaining of transfected cells against acety-lated α-tubulin (Fig. 4B). Moreover, quantitative western blot analysis revealed that FAM161A significantly increased the α-tubulin acetylation levels in 293-EBNA cells (Fig. 4C). In add-ition, bundled microtubules in FAM161A expressing cells were observed to be stable in the presence of 2.5 μM nocodazole
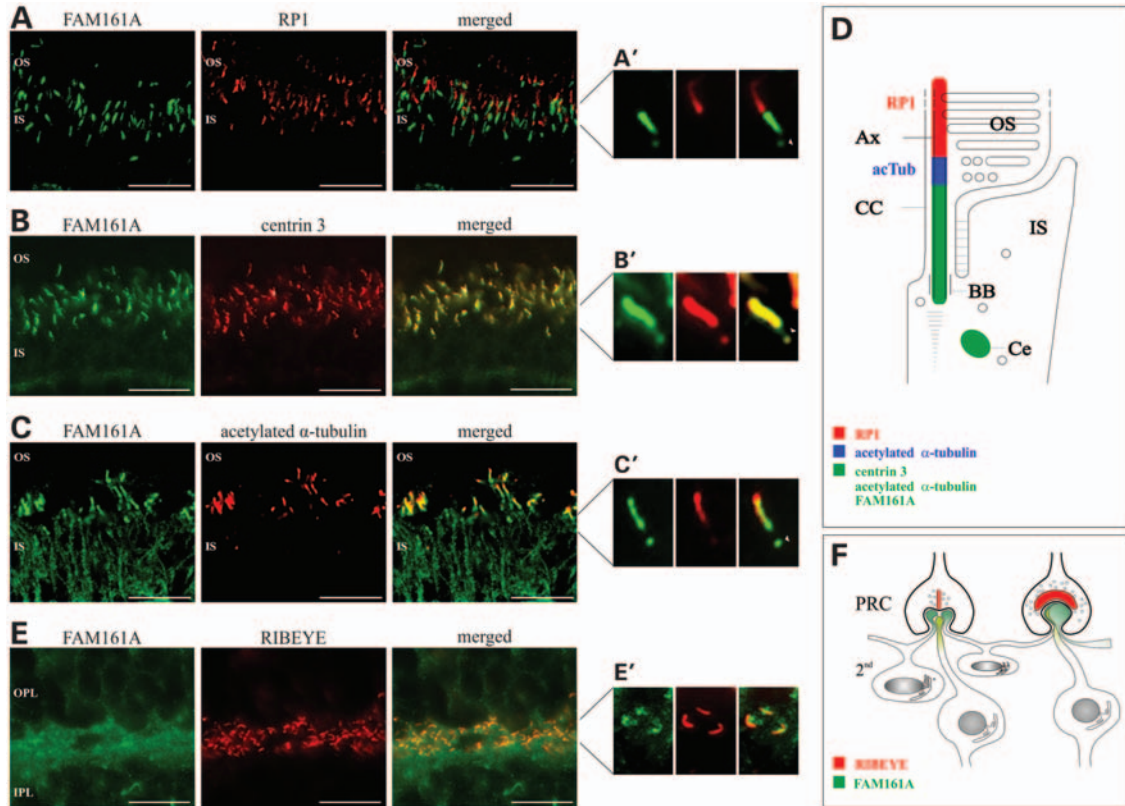
Figure 2. Subcellular localization of FAM161A in the mouse retina. Fluorescent images from the photoreceptor inner/outer segment region simultaneously stained with anti-mFAM161A (green) and (**A**) anti-RP1, (**B**) anti-centrin 3 or (**C**) anti acetylated α-tubulin (all red). (**E**) Fluorescent images from the synaptic region in the OPL double labeled with anti-mFAM161A (green) and RIBEYE (red). Yellow staining in the merged images indicates co-localization. Scale bars, 10 μm. High-magnification images of the ciliary regions of photoreceptors double labeled with antibodies against RP1, centrin 3, acetylated α-tubulin and RIBEYE are shown in A′, B′, C′ and E′. Arrowheads denote adjacent centrioles. Schemes illustrating FAM161A localization in (**D**) ciliary and (**F**) synaptic regions of mouse photoreceptor cells in relation to ciliary and synapse markers are shown on the right. Ax, axoneme; acTub, acetylated alpha-tubulin; CC, connecting cilium; BB, basal body; Ce, centriole; OS, outer segment; IS, inner segment; OPL, outer plexiform layer; IPL, inner plexiform layer. In the ciliary part, FAM161A is present in the connecting cilium, the basal body and the adjacent centriole. In the OPL, FAM161A localizes to post synaptic terminals of second-order neurons.

(Fig. 4B). Ectopic FAM161A co-localized with nocodazole-resistant microtubules but some FAM161A redistributed to the cytoplasm. Treatment of transfected cells with 10 μM nocodazole destabilized the microtubules to a greater extent and increased the FAM161A fraction in the cytosol (Supplementary Material, Fig. S2A), suggesting that FAM161A localization depends on microtubule integrity.

FAM161A undergoes redistribution during mitosis as visualized by double-labeling with anti-α-tubulin antibodies in COS-7 cells transiently transfected with FAM161A (Fig. 4D). At the beginning of cell division, in prophase, FAM161A relocates to the forming mitotic bipolar spindle. As mitosis proceeds through metaphase, anaphase and telophase, FAM161A is present at the spindle poles, astral and spindle microtubules. In telophase and cytokinesis, FAM161A remains located on microtubules nucleated from the centrosome which are involved in the re-formation of the radial interphase array of microtubules. Absence of FAM161A protein, however, was observed on microtubules of the central spindle, indicating that FAM161A is not important for the formation of the midbody and for the stabilization of the cytokinetic furrow.

When overexpressed in LLC-PK1 epithelial cells, FAM161A localized to the cytoplasm in a filamentous-like pattern consistent with microtubule localization (Supplementary Material, Fig. S2B). Co-staining with γ-tubulin, a centrosomal protein required for cell cycle-dependent microtubule nucleation [20] showed that ectopic FAM161A overlapped with γ-tubulin at the microtubule-organizing centers in these cells (Fig. 4E). The FAM161A protein was also detected in primary cilia of LLC-PK1 cells which were visualized by acetylated α-tubulin immunostaining (Fig. 4F). Here, the FAM161A signal was enriched at the cilium base (transition zone/basal body) and weak FAM161A immunoreactivity extended into the proximal ciliary axoneme.

Ectopic FAM161A binds microtubules via its conserved C-terminal domain

To examine which region of FAM161A is important for microtubule localization, deletion mutants were constructed and expressed in COS-7 cells (Fig. 5A). N-terminal truncated enhanced fluorescent green protein (EGFP)-FAM161A_214-660 and EGFP-FAM161A_214-714 containing the alternatively spliced exon 3a of the long isoform were localized at microtubules similar to the full-length short isoform of FAM161A (Fig. 5B). Exon 3a consists of 168 bp encoding 56 amino
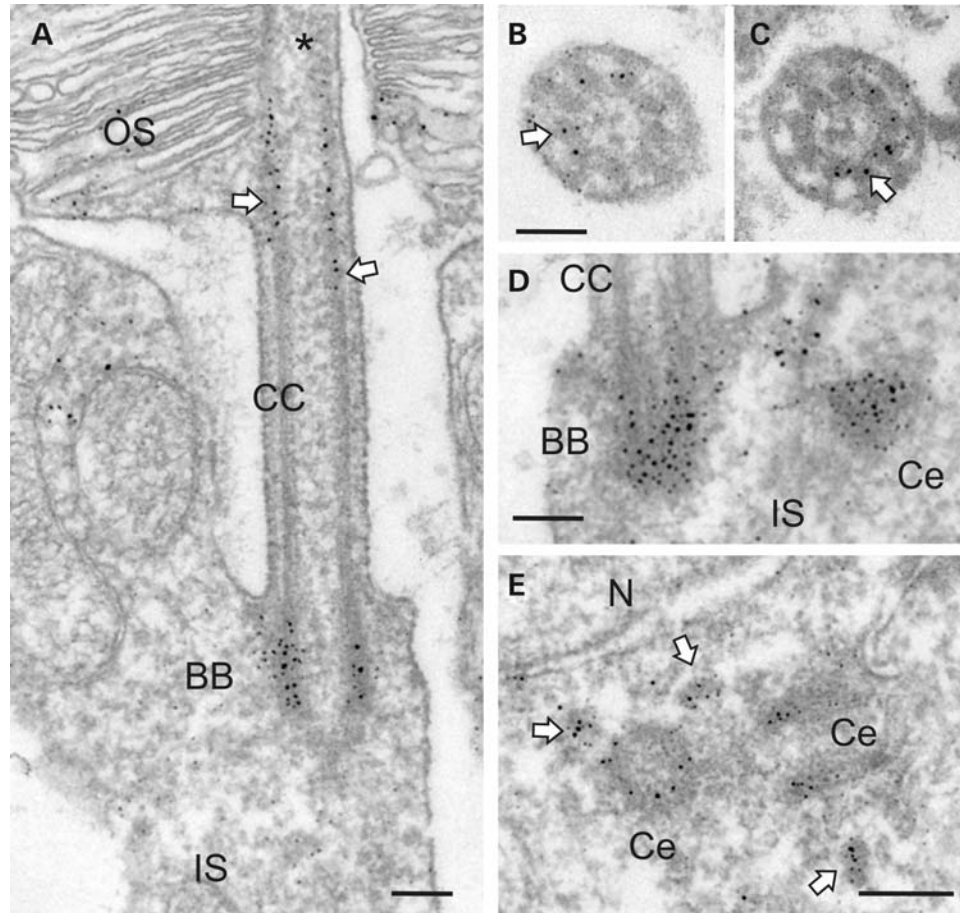
Figure 3. Immunoelectron microscopic localization of FAM161A in retinal photoreceptor cells. (**A**) Electron micrographs of pre-embedding anti-mFAM161A labeling in longitudinal sections through parts of mouse photoreceptor cells. FAM161A is predominantly labeled in the basal body (BB) and the apical connecting cilium (CC) of the rod photoreceptor cell. In the CC, FAM161A is decorated along the microtubule doublets (arrows). The axoneme (asterisk) of the outer segment (OS) is not labeled. The central part of the CC is not labeled due to a lack of epitope accessibility in the pre-embedding labeling protocol (18,19,45). (**B** and **C**) Electron micrographs of anti-mFAM161A labeling in cross-sections through the CC of mouse photoreceptor cells. FAM161A localization is found at the microtubule doublets (arrows). FAM161A is not present in the subciliary compartments of the lumen and the membrane of CC. (**D**) Electron micrographs of anti-mFAM161A labeling in a section through the ciliary base of a mouse rod photoreceptor cell. FAM161A is found at the BB and the adjacent centriole (Ce). (**E**) Electron micrographs of anti-mFAM161A labeling of a centrosome present in the outer nuclear layer of a mouse retina (presumably from a glia cell). In addition to both Ce, centriolar satellites are labeled (arrows). N, nucleus. Scale bars: A, 200 nm; B and C, 150 nm; D, 100 nm; E, 250 nm.

acid residues inserted in the C-terminal part of the conserved UPF0564 domain (Fig. 5A and Supplementary Material, Fig. S3). In contrast, the overexpression of the N-terminal region of FAM161A-1D4 (amino acids 1−285) showed a diffuse cytoplasmic distribution (Fig. 5B). This indicates that the C-terminal portion with the highly conserved UPF0564 domain of both FAM161A isoforms is sufficient to associate with microtubules. Of note, a fraction of overexpressed EGFP-tagged FAM161A fragments accumulated in the nuclei probably due to the presence of the N-terminal EGFP tag (Fig. 5B).

We next studied whether FAM161A interacts with prepolymerized microtubules using *in vitro* microtubule co-sedimentation assays and GST-fusion proteins representing different regions of the FAM161A protein (Fig. 5A). A large quantity of purified GST-FAM161A_230-543 protein containing the minimal UPF0564 domain co-pelleted with taxol-stabilized microtubules, whereas most of GST-FAM161A_1-229 remained in the supernatant fraction (Fig. 5C). These data demonstrate that FAM161A directly binds to microtubules via its conserved C-terminal UPF0564 domain. We also analyzed a possible effect of FAM161A on microtubule dynamics by fluorescence-based tubulin polymerization assays. Tubulin monomers were allowed to polymerize in the presence of different test proteins or drugs at 37°C and the incorporation of a fluorescent reporter was measured by spectrophotometry. As expected, paclitaxel and MAP2 enhanced microtubule assembly, whereas destabilizing nocodazole inhibited tubulin polymerization (Supplementary Material, Fig. S4). In contrast, purified GST-FAM161A_230-543 failed to modulate microtubule formation in these assays (Supplementary Material, Fig. S4).

The conserved C-terminal domain FAM161A mediates homotypic interaction

To investigate FAM161A homotypic protein−protein interaction, GST pull-down assays with several immobilized GST-fusion proteins containing different truncated forms of FAM161A (Fig. 6A) and lysates of 293-EBNA cells
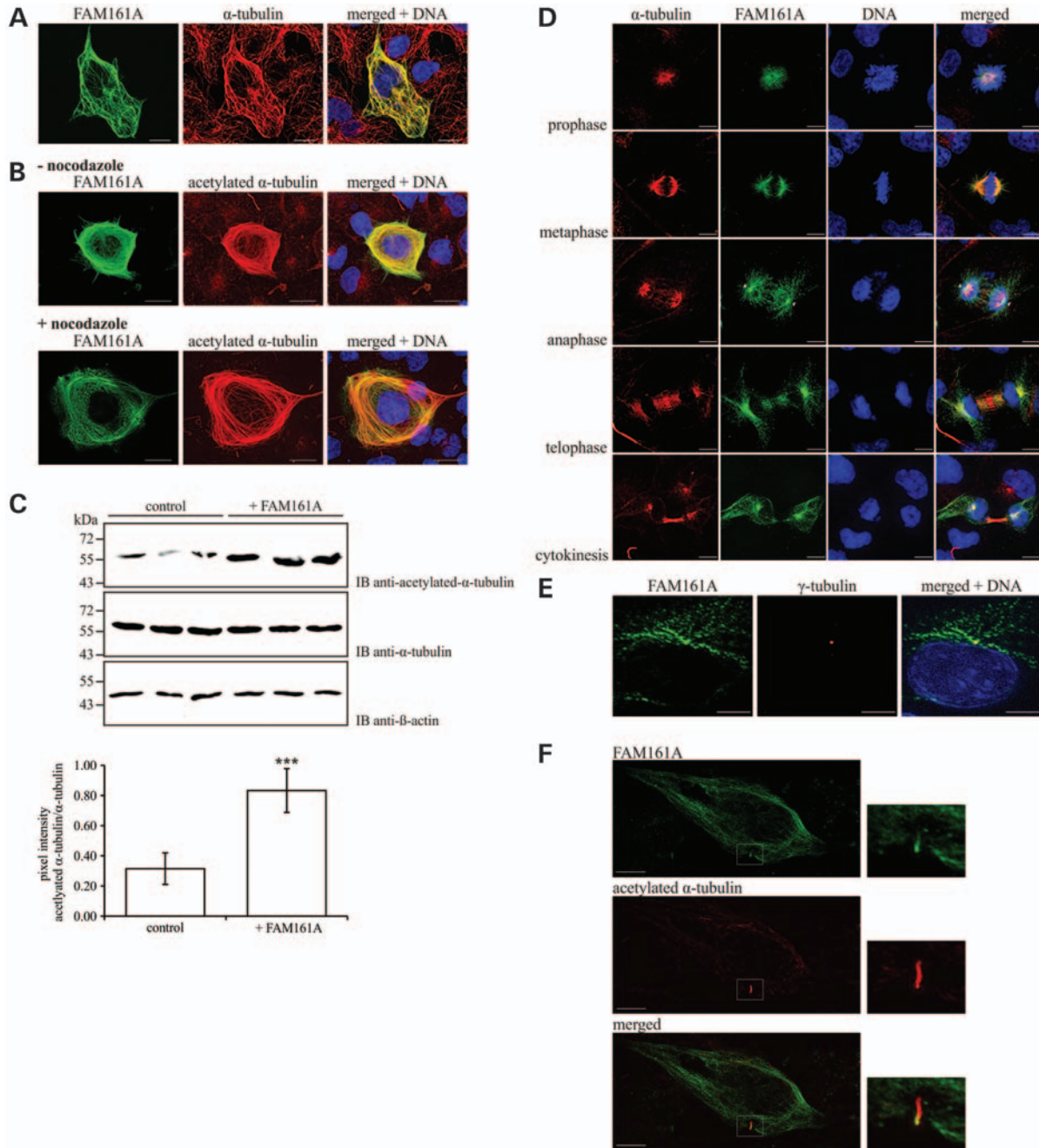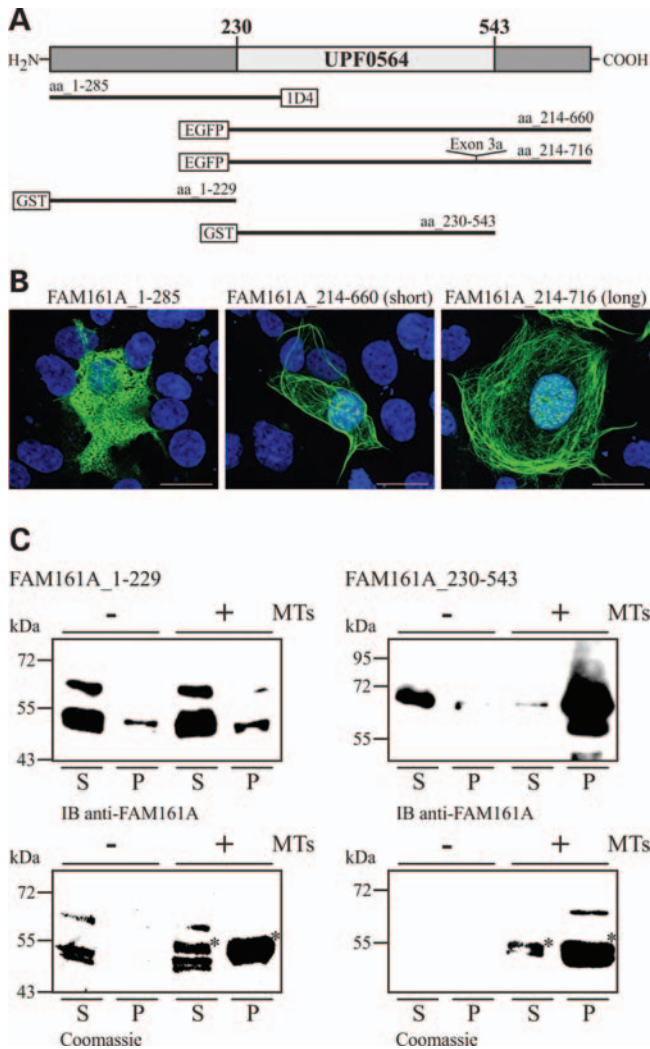
Figure 4. Microtubule localization of FAM161A. (**A**) Co-localization of overexpressed full-length FAM161A (green) and endogenous α-tubulin (red) in COS-7. Scale bar, 10 μm. (**B**) Co-immunostaining of acetylated α-tubulin (red) and FAM161A (green) in FAM161A overexpressing COS-7 cells. In FAM161A-expressing cells, an increase in acetylated α-tubulin is observed and the acetylated α-tubulin is protected against nocodazole treatment. Scale bar, 20 μm. (**C**) Western blots of lysates from 293-EBNA cells transfected with either empty pCEP4.1-1D4 (control) or pCEP4.1-FAM161A-1D4 plasmids in triplicate were labeled with antibodies towards acetylated α-tubulin, α-tubulin and β-actin (as a control for equal loading). Acetylated α-tubulin and α-tubulin immunoreactive bands ($n = 6$ each) were quantified by measuring the pixel intensities and the values were used to calculate the average ratio between acetylated α-tubulin and α-tubulin. FAM161A over-expressing cells showed a statistically significant increase ($P < 0.001$) in α-tubulin acetylation level when compared with control 293-EBNA cells transfected with control vector. (**D**) Co-localization of overexpressed full-length FAM161A (green) and endogenous α-tubulin (red) during cell cycle in COS-7 cells. Arrowheads indicate spindle poles. Scale bar, 10 μm. (**E**) Co-localization of overexpressed full-length FAM161A (green) and endogenous γ-tubulin (red) in LLC-PK1 cells. Scale bar, 5 μm. (**F**) LLC-PK1 cell overexpressing FAM161A (green) was labeled with antibodies against acetylated α-tubulin (red) to visualize primary cilia. Boxed region harboring the primary cilium is shown at a higher magnification on the right. Scale bar, 10 μm. Yellow staining in the merged images indicates co-localization. Nuclei were stained with DAPI.

overexpressing full-length FAM161A were performed. Western blot analysis of proteins eluted from glutathione-sepharose beads showed that GST fused to FAM161A amino acid residues 230–660, 230–543 and 230–386 but not 1–229 or 387–543 bound full-length FAM161A (Fig. 6B). These data indicate that FAM161A_230-386 representing the

Figure 5. FAM161A binds microtubules via its conserved UPF0564 domain. (**A**) Schematic diagram showing the location of the conserved UPF0564 domain of FAM161A, the EGFP-FAM161A deletion constructs and the GST-fusion proteins used to test microtubule binding. (**B**) Fluorescence microscopy of COS-7 cells transiently transfected with FAM161A truncation constructs (green). N-terminal FAM161A_1-285 was detected in the cytoplasm by antibodies toward the Rho1D4 tag. EGFP-FAM161A_214-660 represents the short isoform and EGFP-FAM161A_214-716 represents the long isoform (contains alternatively spliced exon 3a) of FAM161A. Both N-terminally truncated proteins show a cytosolic distribution similar to full-length FAM161A but also accumulate in the nuclei. Nuclei were visualized with DAPI. Scale bar, 20 μm. (**C**) Immunoblot analysis of supernatant (S) and pellet (P) fractions from *in vitro* microtubule co-sedimentation assays with GST-FAM161A-fusion proteins in the presence (+) or the absence (−) of microtubules. FAM161A fragments harboring the conserved UPF0564 domain (FAM161A_230-543) were recovered in the microtubule pellet, whereas N-terminal FAM161A_1-229 remained in the supernatant. Traces of GST-FAM161A_230-543 and a degradation product of GST-FAM161A_1-229 detected in the corresponding pellet fractions in the absence of prepolymerized microtubules may be due to the aggregation of a small fraction of purified fusion proteins. Coomassie stained polyvinylidene difluoride (PVDF) membranes are shown in the bottom row to demonstrate 90% microtubule formation in the pellet (asterisks). Molecular masses are indicated in kDa.

N-terminal half of the UPF0564 domain is necessary and sufficient to mediate the homotypic interaction with full-length FAM161A.

Homotypic FAM161A interaction was independently verified by testing a series of truncated GST-FAM161A and MBP-FAM161A peptides in binding assays (Fig. 6C). MBP-fusion proteins containing the minimal UPF0564 domain (aa-230-543) and partial deletion of the UPF0564 domain (aa-280-413) showed similar ability to bind GST-FAM161A peptides 230–543, 280–413 and 230–386, whereas binding of MBP-FAM161A_230-386 to these GST-fusion proteins was slightly reduced (Fig. 6C). Deletion of the N-terminal portion of the UPF0564 domain (aa_387-543) markedly inhibited or even abolished FAM161A homotypic binding ability. Thus, a minimal region of 107 amino acid residues in the conserved UPF0564 domain (aa_280-386) is critical for homotypic interaction. The protein sequence alignment of UPF0564 domains derived from selected proteins of different species ranging from humans to the ciliate protozoa *Tetrahymena thermophila* revealed a remarkably higher degree of sequence conservation in the N-terminal part of the domain (Supplementary Material, Fig. S3). This includes three stretches of 22–28 amino acid residues predicted to form α-helical structures with high confidence. Inclusion of the three helices in the FAM161A_280-413 fragment appears to increase homotypic binding, suggesting that these secondary structures are crucial elements for homotypic interaction.

FAM161A interacts with FAM161B

To assess whether heterotypic binding between UPF0564 domains of paralogous proteins may occur, we performed co-immunoprecipitation experiments with mammalian cells co-transfected with Flag-FAM161A and FAM161B-1D4 plasmids (Fig. 7A). We first demonstrated the co-immunoprecipitation of FAM161A with polyclonal anti-FAM161B antibodies. Conversely, FAM161B was co-purified from cell extracts when anti-Flag antibodies targeting FAM161A were used for immunoprecipitation. Control experiments with extracts from single-transfected cells confirmed that the co-immunoprecipitation of either molecule mutually depends on each other. Immunofluorescence microscopy of COS-7 cells overexpressing both, FAM161A and FAM161B, showed the co-localization of FAM161A and FAM161B along the microtubule network and supported a physical association of the paralogous proteins (Fig. 7B). GST pull-down assays using truncated GST-FAM161A fusion proteins revealed that overexpressed FAM161B was bound by peptides containing FAM161A amino acid residues 230–660, 230–543 and 230–386 but not 1–229 or 387–543 (Fig. 7C). Thus, the N-terminal part of the UPF0564 domain is responsible for both, homotypic as well as heterotypic protein interactions.

Semi-quantitative reverse transcription polymerase chain reaction (RT−PCR) analysis revealed a high expression of the human *FAM161B* gene in neuronal tissues including the fetal and adult brain, spinal cord and retina (Fig. 7D). Low levels of *FAM161B* transcripts were observed in many other non-neuronal tissues. The *FAM161B* gene localizes to human chromosome 14 band q24.3 and may represent a candidate gene for diseases mapped to this genomic region including primary congenital glaucoma (OMIM 613085).
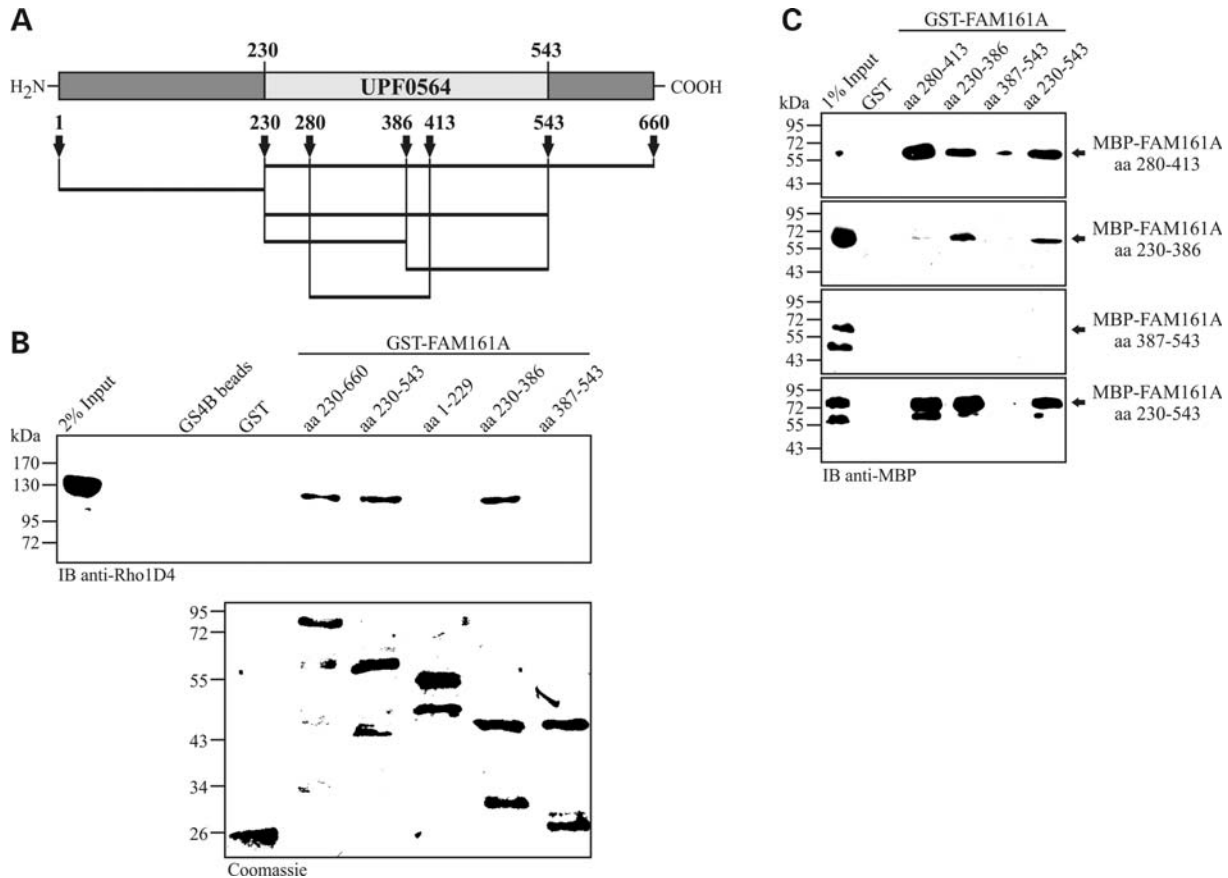
Figure 6. GST pull-down assays to analyze homotypic UPF0564 domain interaction. (**A**) Schematic diagram showing the location of truncated FAM161A proteins used to test homotypic interaction. (**B**) GST-fusion proteins containing truncated FAM161A proteins were incubated with lysates from 293-EBNA cells overexpressing full-length FAM161A-1D4 (input). GST-FAM161A proteins containing the N-terminal half of the UPF0564 domain (amino acids 230−386) bind full-length FAM161A. PVDF-membrane stained with Coomassie shows equal amounts of GST-fusion proteins used in the binding assay. (B and **C**) Bound proteins were identified by immunoblotting with antibodies as indicated below the respective images. GST served as a negative control in GST pull-down assays. (C) GST-FAM161A fragments were mixed with MBP-FAM161A fusion proteins (input) as indicated. GST-FAM161A fusion proteins harboring amino acid residues 230−386, 280−413 and 230−543 bind respective MBP-FAM161A fusion proteins. Interactions between fusion proteins containing the C-terminal half of the UPF0564 domain (amino acids 387−543) and the truncated FAM161A proteins were lacking or were significantly weaker. Expected molecular masses of GST/MBP-fusion proteins: GST-FAM161A: amino acids 1−229, 54 kDa; amino acids 230−386, 46 kDa; amino acids 387−543, 46 kDa; amino acids 280−413, 43 kDa; amino acids 230−543, 64 kDa; amino acids 230−660, 78 kDa; MBP-FAM161A: amino acids 230−386, 61 kDa; amino acids 387−543, 60 kDa; amino acids 280−413, 58 kDa; amino acids 230−543, 79 kDa.

Mapping of amino acid residues critical for homo- and heterotypic protein interaction

The N-terminal 150 amino acids of the UPF0564 domain contain several highly conserved amino acid residues including prolines known to influence protein architecture because of the distinctive cyclic nature of its side chain (Supplementary Material, Fig. S3). Single amino acid substitutions were introduced into several codons (P239A, P241A, P288A, P324A, F327V, P361A and P399A) of GST-FAM161A_230-543 and the mutant fusion proteins were tested for their ability to bind full-length FAM161A or FAM161B (Fig. 8A). Quantification of the signals obtained by western blotting revealed that mutations P288A, F327A and P361A consistently reduced the binding of GST-FAM161A_230-543 to overexpressed FAM161A and FAM161B (Fig. 8B) with significant values obtained for P288A for both FAM161 proteins and for F327A and P361A only for FAM161B. These results indicate that certain positions

in turns of predicted α-helices are most critical for homo- and heterotypic protein interaction.

DISCUSSION

We and others have recently identified *FAM161A* as a novel gene causative for autosomal recessive RP (4,6). The *FAM161A* gene encodes a novel, uncharacterized protein that belongs to an evolutionarily conserved protein family of unknown function. The role of FAM161A in retinal physiology and the pathomechanism leading to retinal degeneration in the absence of FAM161A are unclear.

One important result from the current study is that we discovered an association of endogenous and recombinant FAM161A with microtubules. Microtubules form a dynamic and polarized cytoskeleton and organize themselves into complex structures, such as centrioles, basal bodies and cilia. In photoreceptor
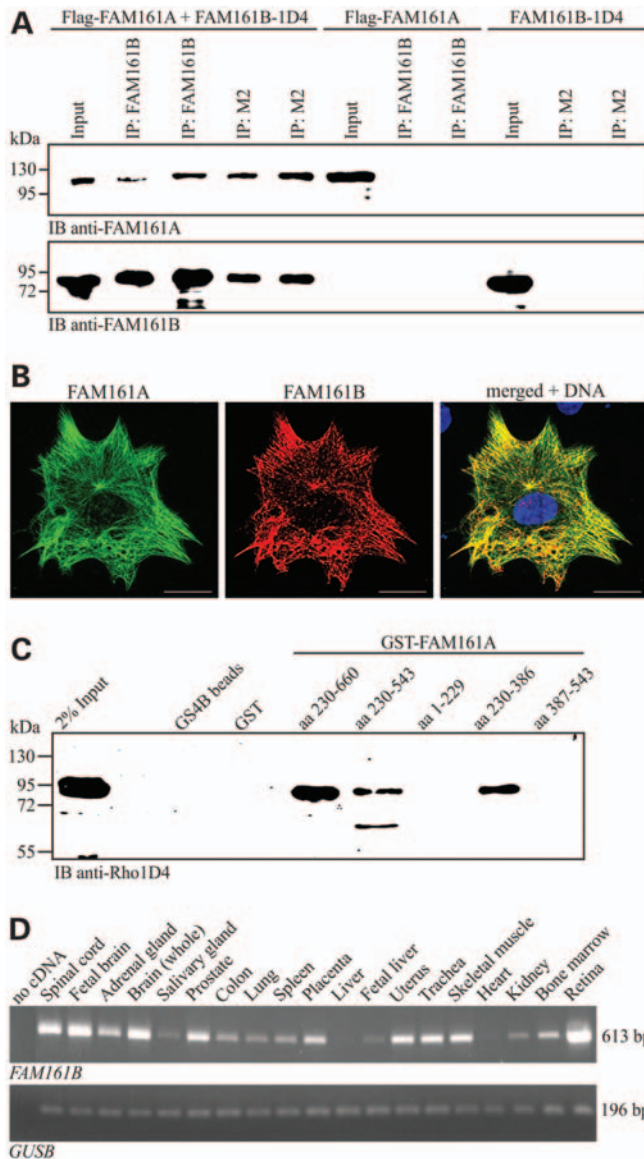
Figure 7. FAM161A interacts with FAM161B. (**A**) Lysates from 293-EBNA cells co-transfected with Flag-FAM161A and FAM161B-1D4 were immunoprecipitated with anti-Flag-M2 affinity gel and anti-FAM161B coupled to protein-A beads. Western blotting of the double-eluted proteins with anti-FAM161A and anti-FAM161B antibodies shows that FAM161B co-immunoprecipitated with FAM161A and vice versa. Cells transfected with either Flag-FAM161A or FAM161B-1D4 alone served as controls. Input was 2% of total cell lysate. (**B**) Immunocytochemistry of COS-7 cells simultaneously transfected with Flag-FAM161A and FAM161B-1D4 expression plasmids. Staining with antibodies against Flag (green) and FAM161B (red) reveals co-localization (yellow) of FAM161A and FAM161B along the cytoplasmic microtubule cytoskeleton. Nuclei were stained with DAPI. Scale bar, 20 μm. (**C**) GST-fusion proteins containing truncated FAM161A proteins were incubated with lysates from 293-EBNA cells overexpressing full-length FAM161B-1D4 (input). GST-FAM161A proteins containing the N-terminal half of the UPF0564 domain (amino acids 230–386) bind full-length FAM161B. GS4B beads and GST served as negative controls. (**D**) Semi-quantitative RT–PCR analysis of *FAM161B* gene expression in 19 human tissues showed ubiquitous expression with varying levels in the different organs. *GUSB* served as a housekeeping gene.

cells, an array of microtubule plus ends grows dynamically out into the inner segment from the microtubule-organizing center nucleated by the basal body and the adjacent centriole at the base of the connecting cilium where the minus ends are tethered (15). Proteins and lipids biosynthesized in the inner segment are delivered from the Golgi apparatus in cargo vesicles along the microtubule cytoskeleton to the base of the connecting cilium. This process involves IFT20, a subunit of the intraflagellar transport (IFT) B subcomplex which has been shown to move from the Golgi apparatus to the ciliary base (21). Furthermore, RP2, a ubiquitously expressed protein linked to severe forms of X-linked RP, is believed to mediate protein transfer from the Golgi to the base of the cilium by regulating Arl3, a small guanosine-5'-triphosphatase (GTPase) (22). We demonstrated that FAM161A is present in the inner segments of mouse photoreceptors by immunofluorescence analysis (4) (present study). We also show that FAM161A associates with the cytoplasmic microtubule cytoskeleton *in vitro* supporting a role of FAM161A in sorting or trafficking of proteins along cytoplasmic microtubules in the inner segment. Immunoelectron microscopy, however, failed to detect substantial amounts of FAM161A along microtubule tracks. The observation that the extent of FAM161A immunoreactivity in the inner segments varies among different microscopy techniques and applied fixation protocols may reflect differences in the stability or accessibility of the FAM161A antigen. Further studies are required to clarify this discrepancy.

Both immunofluorescence and immunoelectron microscopy consistently demonstrated a predominant presence of endogenous FAM161A in the connecting cilium, basal body and adjacent centriole of photoreceptors. Moreover, ectopic FAM161A was found in centrosomes and at the base of the primary cilium in cultured cells. The connecting cilium of photoreceptors is the structural equivalent to the transition zone of primary cilia. It is involved in the establishment of a barrier to membrane diffusion and serves as a gate for proteins destined for the ciliary transport (23). Although direct binding of endogenous FAM161A with microtubules needs to be verified, the observation that FAM161A is closely associated with the microtubule doublets in the connecting cilium suggests that FAM161A directly interacts with the ciliary microtubule tracks. Thus, besides the retina-specific RP1 protein that associates with axonemal microtubules in the outer segments (24), FAM161A is the second RP causing protein that interacts with the microtubule cytoskeleton. Transport through the cilium and further apical along axonemal microtubules is believed to be mediated by a conserved IFT mechanism (19,25), initially identified in *Chlamydomonas* (26). In photoreceptors, KIF17 and kinesin-II family motors drive the plus end-directed transport of proteins and membrane vesicles, whereas cytoplasmic dynein 1 and 2 power transport toward the microtubule minus end (27,28). Small GTPases like the Rab protein family as well as other mechanisms like mitogen-activated protein kinase cascades regulate directional intracellular transport through the organization of macromolecular complexes, motor localization and cytoskeleton remodeling (29). Thus, FAM161A in photoreceptors might act in addition
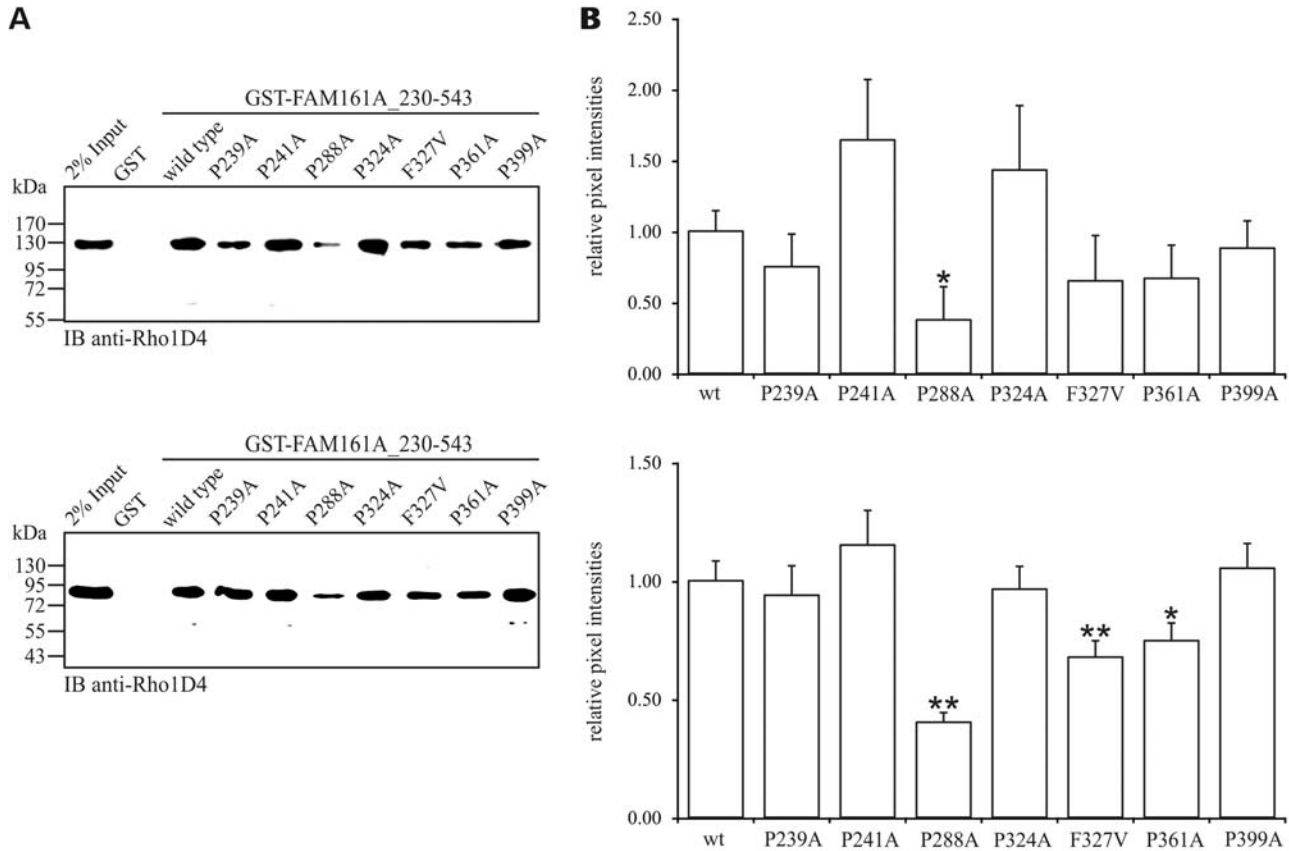
Figure 8. Amino acid substitution to identify key residues within the UPF0564 domain. (**A**) GST pull-down assay performed with GST-fusion proteins containing the wild-type or different mutated UPF0564 domains of FAM161A and lysates from 293-EBNA cells overexpressing full-length FAM161A-1D4 or FAM161B-1D4 (input). (**B**) Bands were quantified by measuring the pixel intensities and normalized to the 2% input. Relative abundance of each band was calculated by comparing the averaged values to wild-type ($n = 3$). Mutations P288A, F327A and P361A consistently reduced the binding of GST-FAM161A_230-543 to overexpressed FAM161A and FAM161B with significant values obtained for P288A for both FAM161 proteins and for F327A and P361A only for FAM161B. Significant differences between average pixel intensities are indicated with an asterisk ($^*P < 0.05$, $^{**}P < 0.01$, Student's t-test).

or in concert with these or other factors to contribute to the microtubule-mediated intraciliary protein translocation from the periciliary compartment to the base of the outer segment.

Overexpression of FAM161A in cultured cells confers drug stability to microtubules and causes an increased level of α-tubulin acetylation. Acetylation is generally considered to occur on stable microtuble assemblies but it is as yet unclear whether this posttranslational modification is the cause of microtubule stability. Several microtubule-associated proteins (MAPs) are known to induce microtubule acetylation and stability (30), including RP1 whose activity appears to be regulated by ciliary male germ cell-associated kinase (31). With the discovery of acetylation sites exposed on the outer surface of microtubules (32), it has become conceivable that an interaction between microtubules and MAPs including FAM161A might directly control the modification of these sites. Alternatively, FAM161A could modify the acetylation status of microtubules by binding to tubulin acetylating/deacetylating enzymes (e. g. HDAC6, αTAT1) (33,34) as was shown for other proteins like TPPP/p25 or dysferlin (35,36). Acetylation and/or deacetylation regulators are important in the assembly and disassembly of cilia. The BBS4-interacting protein BBIP10, for example, couples the acetylation of axonemal microtubules to ciliary membrane growth (37). In addition,

acetylation was shown to selectively stimulate microtubule binding of molecular motors (38,39), indicating an effect on intracellular transport processes. Axonemal microtubules along the connecting cilium including the basal body are highly stable structures (40). FAM161A appears to contribute to microtubule stability and might therefore be of importance to maintain the microtubule tracks that are essential for intraciliary transport and survival of the photoreceptor sensory cilium. Further studies are now required to elucidate the mechanism by which FAM161A confers microtubule stability and to clarify a possible role in the regulation of post-translational modification of tubulin.

FAM161A was also shown to be present in retinal synaptic layers and the ganglion cell layer suggesting that this molecule participates in the maintenance of microtubule tracks or execution of microtubule-dependent functions in non-photoreceptors. In the outer plexiform layer, FAM161A was found post-synaptic to the ribbon synapses in retinal second-order neurons similar to some IFT complex B proteins and the KIF17 motor (19,41). Taken together, we would therefore hypothesize that loss of FAM161A results in mislocalization and accumulation of cargo vesicles in the inner segment as well as disturbed synaptic transmission ultimately causing retinal cell degeneration.

FAM161A is a member of the uncharacterized protein family UPF0564 of unknown function which shows no

significant sequence similarities with known microtubule-associated proteins. We found that the evolutionary conserved UPF0564 domain mediates the interaction of FAM161A with microtubules. The UPF0564 domain is composed of a remarkable large number of basic amino acids ($pI = 9.8$) that can potentially interact with the acidic tubulin surface. Similar to FAM161A, its closest relative, FAM161B, also co-localizes with the microtubule network, suggesting that the uncharacterized protein family UPF0564 represents a novel family of microtubule-associated proteins.

Besides microtubule binding, the UPF0564 domain allows intermolecular interactions between FAM161 family members and thus implies scaffolding function. Microtubule-binding domains that also enable multimerization are known in other proteins. The catalytic subunit of *Arabidopsis thaliana* katanin has a microtubule-stimulated ATPase activity to sever microtubules and contains a microtubule-binding motif that participates in the formation of ring-shaped oligomers (42). The conformation of the N-terminal part of the UPF0564 domain determined by predicted right-handed α-helices is crucial for protein interaction; however, more detailed structural data are required to understand how UPF0564 domain subunits assemble into di- or multimers. Moreover, the dynamics of microtubule-binding versus intermolecular interactions of the UPF0564 domain need to be determined. It is possible that the N-terminus of FAM161 proteins with an as yet unknown function is involved in the regulation of these processes.

Taken together, the present study provides new insights into the molecular properties of FAM161A and related proteins of the UPF0564 family. The ongoing characterization of FAM161A and the establishment of animal models should soon help to understand the precise role of FAM161A in the retina and the pathomechanism leading to FAM161A-associated retinal degeneration.

MATERIAL AND METHODS

DNA constructs

Constructs for the bacterial expression of GST- and MBP-fusion proteins of human FAM161A were prepared by RT–PCR from human or mouse retinal RNA and introduced into the pGEX4T3 (Amersham Biosciences, Piscataway, NJ, USA) or pMAL-c2 (New England Biolabs, Beverly, MA, USA) vectors. Constructs contained the following amino acid residues: GST-FAM161A amino acids 1–229, GST-FAM161A amino acids 14–355, GST-FAM161A amino acids 230–386, GST-FAM161A amino acids 387–543, GST-FAM161A amino acids 280–413, GST-FAM161A amino acids 230–543, GST-FAM161A amino acids 230–660, MBP-FAM161A amino acids 14–355, MBP-FAM161A amino acids 230–386, MBP-FAM161A amino acids 387–543, MBP-FAM161A amino acids 280–413 and MBP-FAM161A amino acids 230–543. The P239A, P241A, P288A, P324A, F327V, P361A and P399A mutations were introduced into GST-FAM161A amino acids 230–543 by PCR-based site-directed mutagenesis using complementary primers. The expression and purification of fusion proteins was performed as described previously (43).

For expression in mammalian cells, full-length FAM161A and FAM161B cDNAs were PCR-amplified using DKFZp686O21143Q and IRATp970A0180D cDNA clones (obtained from imaGenes GmbH, Berlin, Germany) as templates and either inserted into the pCEP4.1 vector in-frame with a C-terminal Rho 1D4 tag (TETSQVAPA) (44) or the pFLAG-CMV4 vector in-frame with a N-terminal Flag tag (Sigma-Aldrich, St Louis, MO, USA). Truncation constructs FAM161A amino acids 1–285 in pCEP4.1-1D4, EGFP-FAM161A amino acids 214–660 and EFGFP-FAM161A amino acids 214–716 in pEGFP-C1 (BD Biosciences, San Jose, CA, USA) were subcloned from the full-length FAM161A construct or amplified from human retina RNA by RT–PCR. All constructs were verified by direct sequencing. The nucleotide sequences of the primers used for cloning are provided upon request. Transfection of 293-EBNA, LLC-PK1 or COS-7 cells was performed with the *Trans*IT-LT1 transfection reagent (Mirus Bio, Madison, WI, USA) following the manufacturer's instructions. Protein concentrations of cell lysates were determined by Bradford assay (Roti-quant®; Roth, Karlsruhe, Germany).

Antibodies

A polyclonal anti-mFAM161A antiserum (mFAM161A) was generated by immunizing rabbits with GST-mFAM161A amino acids 14–355 fusion protein (Davids Biotechnology, Regensburg, Germany) and affinity-purified using HiTrap NHS-

activated sepharose HP columns as described previously (43). Antibodies against human FAM161A (hFAM161A), FAM161B, α-tubulin, γ-tubulin, acetylated α-tubulin, β-actin and Flag (M2) were purchased from Sigma-Aldrich. Monoclonal antibodies to centrin-3 were used as a molecular marker for the ciliary apparatus of photoreceptors (14). Monoclonal mouse antibodies to RIBEYE (=CtBP2) were purchased from BD Biosciences (Heidelberg, Germany). Monoclonal antibodies against rhodopsin (Rho 1D4) and RS1 were kindly provided by R. Molday (UBC, Vancouver, BC, Canada), polyclonal chicken anti-RP1 antibodies were a gift from E. Pierce (University of Pennsylvania, Philadelphia, PA, USA). Secondary antibodies conjugated to horseradish peroxidase were purchased from Calbiochem (La Jolla, CA, USA), and IgGs conjugated to Alexa 488, Alex 568 and Alexa 594 were from Invitrogen (La Jolla, CA, USA).

Immunofluorescence labeling

Immunohistochemistry of mouse and human retinal cryosections was performed as described elsewhere (43). To evaluate the specificity of the antibody, 100 μl of diluted affinity-purified antibody was preadsorbed for 4 h with 100 μg of MBP-mFAM161A fusion protein immobilized on amylose resins. The beads were pelleted at 1000*g* for 3 min and the supernatants were used for labeling. Immunocytochemistry was done on cells seeded on poly-L-lysine (0.1 mg/ml)- or collagen (1 mg/ml)-coated glass coverslips and fixed with microtubule preserving buffer [0.1 M *N*-(2-hydroxyethyl)piperazine-*N'*-(2-ethanesulfonic acid), 2% PFA, 4% sucrose, 0.5% Triton X-100, 4% polyethylglycol, 4 mM ethylene glycol-bis(2-aminoethylether)-*N,N,N',N'*-tetraacetic acid (EGTA), 1 mM $MgCl_2$]. To analyze microtubule stabilization, COS-7 cells overexpressing

FAM161A were incubated with medium containing nocodazole for 2 h at 37°C and fixed. Labeled species were examined under an LSM 710 laser scanning microscope (Zeiss, Jena, Germany) or were viewed under an AxioImager motorized microscope with Apotome attachment (Zeiss). Image processing was achieved with the Axiovision software with integrated Z-stack and extended focus modules (Zeiss).

Immunoelectron microscopy

For immunoelectron microscopy, we followed the previously published protocol (18,19,45). After washing with phosphate buffered saline (PBS), biotinylated secondary antibodies were applied to the sections. After PBS washes, antibody reactions were visualized by a Vectastain ABC-Kit (Vector Laboratories) and adding 0.01% hydrogen peroxide to 0.05 M diaminobenzidine (DAB) solution. Stained retinas were fixed in 2.5% glutaraldehyde in 0.1 M cacodylate buffer (pH 7.4), and DAB precipitates were silver enhanced followed by post-fixation in cacodylate buffered 0.5% OsO_4 on ice. Dehydrated specimens were flat-mounted between two sheaths of ACLAR®-films (Ted Pella Inc., Redding, USA) in Araldite® resin. Ultrathin sections were analyzed in a Tecnai 12 BioTwin transmission electron microscope (FEI, Eindhoven, the Netherlands). Images were obtained with a CCD camera (SIS Megaview3, Herzogenrath, Germany) acquired by ana-lSIS® (Soft Imaging System, Münster, Germany) and processed with Adobe Photoshop CS (Adobe Systems).

Microtubule-binding protein spin-down assay

The *in vitro* microtubule co-sedimentation potential of FAM161A was analyzed using the microtubule-binding protein spin-down assay kit (Cytoskeleton Inc., Denver, CO, USA) according to the manufacturer's recommendations. Briefly, microtubules were assembled from bovine brain tubulin (purity >99%) for 20 min at 35°C and stabilized by the addition of taxol (20 μM). Stable microtubules (9 μg) were then incubated with 2 μg of GST-fusion proteins for 30 min at room temperature in PEM buffer (80 mM PIPES, pH 6.9, 1 mM EGTA, 1 mM $MgCl_2$) in a total volume of 50 μl. MAP2 and bovine serum albumin were used as positive and negative controls, respectively. The microtubule/protein mixtures were added to 100 μl of cushion puffer (80 mM PIPES 7.0, 1 mM EGTA, 1 mM $MgCl_2$, 60% glycerol) and microtubules were pelleted by centrifugation at 100 000g for 40 min at room temperature. The uppermost layer (50 μl) of the supernatant and the pellet was mixed with Laemmli sample buffer and analyzed by immunoblotting.

Tubulin polymerization assay

The effect of FAM161A on tubulin polymerization was analyzed with the fluorescence-based tubulin polymerization assay kit (Cytoskeleton Inc.). Fluorescence emission at 460 nm (excitation 355 nm) is enhanced as a function of the insertion of the fluorescent reporter 4′,6-diamidino-2-phenylindole into polymerizing microtubules. Polymerization was monitored at 37°C with a FLUOstar OPTIMA spectrophotometer (BMG Labtech GmbH, Ortenberg, Germany). In the enhancer detection mode, purified bovine brain tubulin (purity >99) was diluted in buffer 1 (80 mM PIPES, pH 6.9, 0.5 mM EGTA, 2.0 mM $MgCl_2$, 10 μM fluorescent reporter) to a final concentration of 2 mg/ml and supplemented with 1 mM GTP. The inhibitor detection mode was performed by the addition of 20% v/v glycerol to buffer 1. After addition of the tubulin mixture to 5 μl of GST-fusion proteins (1 mg/ml), the fluorescence signal was measured every 60 s for 60 min. Paclitaxel (30 μM) and MAP2 protein (1 mg/ml) were used as positive controls known to enhance tubulin polymerization. Nocodazole (30 μM) served as positive control known to inhibit tubulin polymerization.

GST pull-down assays

GST pull-down assays were performed with 293-EBNA cell lysates overexpressing FAM161A or FAM161B and analyzed by western blotting as described previously (43). To test interaction between GST- and MBP-fusion proteins, 7.5 μg of purified GST-fusion proteins were incubated with equal amounts of MBP-fusion proteins together with pre-washed glutathione sepharose 4B beads in a total volume of 300-μl TNBN buffer (50 mM Tris–HCl, pH 8.0, 200 mM NaCl, 15 mM 2-mercaptoethanol, 0.1% Nonidet P-40) at 4°C for 1 h. Bound proteins were eluted from the beads by incubation with Laemmli sample buffer and subjected to western blot analysis using mouse anti-MBP antibodies. Pixel intensities of the bands were quantified with TotalLab TL100 (v2006) software (Nonlinear Dynamics Ltd, Newcastle upon Tyne, UK). Statistical analysis ($n = 3$) was performed using the Student's t-test with $P = 0.05$ as the level of significance.

Immunoprecipitation

Triton X-100-solubilized lysates of 293-EBNA cells co-transfected with Flag-FAM161A and FAM161B-1D4 constructs were mixed with either anti-Flag M2 affinity gel (Sigma-Aldrich) or anti-FAM161B antibodies followed by the addition of protein A-sepharose 4B (Sigma-Aldrich) and incubated for 1 h at 4°C. After three washes with PBS/0.1% Triton X-100, the immunoprecipitates were boiled in Laemmli sample buffer and analyzed by western blotting.

RNA expression analysis

The human total RNA master panel was purchased from BD Biosciences Clontech (Palo Alto, CA, USA). Total RNA from human retina was isolated as described (43). RT–PCR was performed with primer pair FAM161B_F3 (5′-CCCTC TCTGCCAACACTCTC-3′) and FAM161B_*Xho*I_R (5′-CTCGAGGCAAGTGATACGAGATTTTCTG-3′), the constitutively expressed housekeeper gene *GUSB* was used as a control for RNA integrity.

Bioinformatics

Homologous amino acid sequences of FAM161A were obtained from Pfam (http://www.sanger.ac.uk/) and by Psi-BLAST database searches (http://blast.ncbi.nlm.nih.gov/). Multiple sequence alignment was performed with MAFFT (46) using the

E-INS-i method. Protein secondary structure prediction was done on the basis of the alignment of the conserved UPF0564 domain on the Jpred 3 server (47).

SUPPLEMENTARY MATERIAL

Supplementary Material is available at *HMG* online.

ACKNOWLEDGEMENTS

FUNDING

REFERENCES

1. Ayuso, C. and Millan, J.M. (2010) Retinitis pigmentosa and allied conditions today: a paradigm of translational research. *Genome Med.*, **2**, 34.
2. Insinna, C. and Besharse, J.C. (2008) Intraflagellar transport and the sensory outer segment of vertebrate photoreceptors. *Dev. Dyn.*, **237**, 1982–1992.
3. Adams, N.A., Awadein, A. and Toma, H.S. (2007) The retinal ciliopathies. *Ophthalmic Genet.*, **28**, 113–125.
4. Langmann, T., Di Gioia, S.A., Rau, I., Stöhr, H., Maksimovic, N.S., Corbo, J.C., Renner, A.B., Zrenner, E., Kumaramanickavel, G., Karlstetter, M. *et al.* (2010) Nonsense mutations in FAM161A cause RP28-associated recessive retinitis pigmentosa. *Am. J. Hum. Genet.*, **87**, 376–381.
5. Gu, S., Kumaramanickavel, G., Srikumari, C.R., Denton, M.J. and Gal, A. (1999) Autosomal recessive retinitis pigmentosa locus RP28 maps between D2S1337 and D2S286 on chromosome 2p11-p15 in an Indian family. *J. Med. Genet.*, **36**, 705–707.
6. Bandah-Rozenfeld, D., Mizrahi-Meissonnier, L., Farhy, C., Obolensky, A., Chowers, I., Pe'er, J., Merin, S., Ben-Yosef, T., Ashery-Padan, R., Banin, E. and Sharon, D. (2010) Homozygosity mapping reveals null mutations in FAM161A as a cause of autosomal-recessive retinitis pigmentosa. *Am. J. Hum. Genet.*, **87**, 382–391.
7. Li, S., Armstrong, C.M., Bertin, N., Ge, H., Milstein, S., Boxem, M., Vidalain, P.O., Han, J.D., Chesneau, A., Hao, T. *et al.* (2004) A map of the interactome network of the metazoan *C. elegans*. *Science*, **303**, 540–543.
8. Gómez-Baldó, L., Schmidt, S., Maxwell, C.A., Bonifaci, N., Gabaldón, T., Vidalain, P.O., Senapedis, W., Kletke, A., Rosing, M., Barnekow, A. *et al.* (2010) TACC3-TSC2 maintains nuclear envelope structure and controls cell division. *Cell Cycle*, **9**, 1143–1155.
9. Liu, Q., Tan, G., Levenkova, N., Li, T., Pugh, E.N. Jr., Rux, J.J., Speicher, D.W. and Pierce, E.A. (2007) The proteome of the mouse photoreceptor sensory cilium complex. *Mol. Cell Proteomics*, **6**, 1299–1317.
10. Jakobsen, L., Vanselow, K., Skogs, M., Toyoda, Y., Lundberg, E., Poser, I., Falkenby, L.G., Bennetzen, M., Westendorf, J., Nigg, E.A. *et al.* (2011) Novel asymmetrically localizing components of human centrosomes identified by complementary proteomics methods. *EMBO J.*, **30**, 1520–1535.
11. Liu, Q., Zhou, J., Daiger, S.P., Farber, D.B., Heckenlively, J.R., Smith, J.E., Sullivan, L.S., Zuo, J., Milam, A.H. and Pierce, E.A. (2002) Identification and subcellular localization of the RP1 protein in human and mouse photoreceptors. *Invest. Ophthalmol. Vis. Sci.*, **43**, 22–32.
12. Horst, C.J., Johnson, L.V. and Besharse, J.C. (1990) Transmembrane assemblage of the photoreceptor connecting cilium and motile cilium transition zone contain a common immunologic epitope. *Cell Motility and the Cytoskeleton*, **17**, 329–344.
13. Hong, D.H., Pawlyk, B., Sokolov, M., Strissel, K.J., Yang, J., Tulloch, B., Wright, A.F., Arshavsky, V.Y. and Li, T. (2003) RPGR isoforms in photoreceptor connecting cilia and the transitional zone of motile cilia. *Invest. Ophthalmol. Vis. Sci.*, **44**, 2413–2421.
14. Trojan, P., Krauss, N., Choe, H.W., Giessl, A., Pulvermüller, A. and Wolfrum, U. (2008) Centrins in retinal photoreceptor cells: regulators in the connecting cilium. *Prog. Retin. Eye Res.*, **27**, 237–259.
15. Troutt, L.L., Wang, E., Pagh-Roehl, K. and Burnside, B. (1990) Microtubule nucleation and organization in teleost photoreceptors: microtubule recovery after elimination by cold. *J. Neurocytol.*, **19**, 213–223.
16. tom Dieck, S., Altrock, W.D., Kessels, M.M., Qualmann, B., Regus, H., Brauner, D., Fejtová, A., Bracko, O., Gundelfinger, E.D. and Brandstätter, J.H. (2005) Molecular dissection of the photoreceptor ribbon synapse: physical interaction of Bassoon and RIBEYE is essential for the assembly of the ribbon complex. *J. Cell Biol.*, **168**, 825–836.
17. Overlack, N., Kilic, D., Bauss, K., Märker, T., Kremer, H., van Wijk, E. and Wolfrum, U. (2011) Direct interaction of the Usher syndrome 1G protein SANS and myomegalin in the retina. *Biochim. Biophys. Acta*, **1813**, 1883–1892.
18. Sedmak, T., Sehn, E. and Wolfrum, U. (2009) Immunoelectron microscopy of vesicle transport to the primary cilium of photoreceptor cells. *Methods Cell Biol.*, **94**, 259–272.
19. Sedmak, T. and Wolfrum, U. (2010) Intraflagellar transport molecules in ciliary and nonciliary cells of the retina. *J. Cell Biol.*, **189**, 171–186.
20. Joshi, H.C., Palacios, M.J., McNamara, L. and Cleveland, D.W. (1992) Gamma-tubulin is a centrosomal protein required for cell cycle-dependent microtubule nucleation. *Nature*, **356**, 80–83.
21. Follit, J.A., Tuft, R.A., Fogarty, K.E. and Pazour, G.J. (2006) The intraflagellar transport protein IFT20 is associated with the Golgi complex and is required for cilia assembly. *Mol. Biol. Cell*, **17**, 3781–3792.
22. Evans, R.J., Schwarz, N., Nagel-Wolfrum, K., Wolfrum, U., Hardcastle, A.J. and Cheetham, M.E. (2010) The retinitis pigmentosa protein RP2 links pericentriolar vesicle transport between the Golgi and the primary cilium. *Hum. Mol. Genet.*, **19**, 1358–1367.
23. Czarnecki, P.G. and Shah, J.V. (2012) The ciliary transition zone: from morphology and molecules to medicine. *Trends Cell Biol.*, **22**, 201–210.
24. Liu, Q., Zuo, J. and Pierce, E.A. (2004) The retinitis pigmentosa 1 protein is a photoreceptor microtubule-associated protein. *J. Neurosci.*, **24**, 6427–6436.
25. Rosenbaum, J.L. and Witman, G.B. (2002) Intraflagellar transport. *Nat. Rev. Mol. Cell Biol.*, **3**, 813–825.
26. Kozminski, K.G., Johnson, K.A., Forscher, P. and Rosenbaum, J.L. (1993) A motility in the eukaryotic flagellum unrelated to flagellar beating. *Proc. Natl Acad. Sci. USA*, **90**, 5519–5523.
27. Scholey, J.M. (2008) Intraflagellar transport motors in cilia: moving along the cell's antenna. *J. Cell Biol.*, **180**, 23–29.
28. Insinna, C., Humby, M., Sedmak, T., Wolfrum, U. and Besharse, J.C. (2009) Different roles for KIF17 and kinesin II in photoreceptor development and maintenance. *Dev. Dyn.*, **238**, 2211–2222.
29. Caviston, J.P. and Holzbaur, E.L. (2006) Microtubule motors at the intersection of trafficking and transport. *Trends Cell Biol.*, **16**, 530–537.
30. Takemura, R., Okabe, S., Umeyama, T., Kanai, Y., Cowan, N.J. and Hirokawa, N. (1992) Increased microtubule stability and alpha tubulin acetylation in cells transfected with microtubule-associated proteins MAP1B, MAP2 or tau. *J. Cell Sci.*, **103**, 953–964.
31. Omori, Y., Chaya, T., Katoh, K., Kajimura, N., Sato, S., Muraoka, K., Ueno, S., Koyasu, T., Kondo, M. and Furukawa, T. (2010) Negative regulation of ciliary length by ciliary male germ cell-associated kinase (Mak) is required for retinal photoreceptor survival. *Proc. Natl Acad. Sci. USA*, **107**, 22671–22676.
32. Choudhary, C., Kumar, C., Gnad, F., Nielsen, M.L., Rehman, M., Walther, T.C., Olsen, J.V. and Mann, M. (2009) Lysine acetylation targets protein complexes and co-regulates major cellular functions. *Science*, **325**, 834–840.

33. Hubbert, C., Guardiola, A., Shao, R., Kawaguchi, Y., Ito, A., Nixon, A., Yoshida, M., Wang, X.F. and Yao, T.P. (2002) HDAC6 is a microtubule-associated deacetylase. *Nature*, **417**, 455–458.

34. Shida, T., Cueva, J.G., Xu, Z., Goodman, M.B. and Nachury, M.V. (2010) The major alpha-tubulin K40 acetyltransferase alphaTAT1 promotes rapid ciliogenesis and efficient mechanosensation. *Proc. Natl Acad. Sci. USA*, **107**, 21517–21522.

35. Tőkési, N., Lehotzky, A., Horváth, I., Szabó, B., Oláh, J., Lau, P. and Ovádi, J. (2010) TPPP/p25 promotes tubulin acetylation by inhibiting histone deacetylase 6. *J. Biol. Chem.*, **285**, 17896–17906.

36. Di Fulvio, S., Azakir, B.A., Therrien, C. and Sinnreich, M. (2011) Dysferlin interacts with histone deacetylase 6 and increases alpha-tubulin acetylation. *PLoS One*, **6**, e28563.

37. Loktev, A.V., Zhang, Q., Beck, J.S., Searby, C.C., Scheetz, T.E., Bazan, J.F., Slusarski, D.C., Sheffield, V.C., Jackson, P.K. and Nachury, M.V. (2008) A BBSome subunit links ciliogenesis, microtubule stability, and acetylation. *Dev. Cell.*, **15**, 854–865.

38. Reed, N.A., Cai, D., Blasius, T.L., Jih, G.T., Meyhofer, E., Gaertig, J. and Verhey, K.J. (2006) Microtubule acetylation promotes kinesin-1 binding and transport. *Curr. Biol.*, **16**, 2166–2172.

39. Dompierre, J.P., Godin, J.D., Charrin, B.C., Cordelières, F.P., King, S.J., Humbert, S. and Saudou, F. (2007) Histone deacetylase 6 inhibition compensates for the transport deficit in Huntington's disease by increasing tubulin acetylation. *J. Neurosci.*, **27**, 3571–3583.

40. Arikawa, K. and Williams, D.S. (1993) Acetylated alpha-tubulin in the connecting cilium of developing rat photoreceptors. *Invest. Ophthalmol. Vis. Sci.*, **34**, 2145–2149.

41. Kayadjanian, N., Lee, H.S., Piña-Crespo, J. and Heinemann, S.F. (2007) Localization of glutamate receptors to distal dendrites depends on subunit composition and the kinesin motor protein KIF17. *Mol. Cell. Neurosci.*, **34**, 219–230.

42. Stoppin-Mellet, V., Gaillard, J., Timmers, T., Neumann, E., Conway, J. and Vantard, M. (2007) Arabidopsis katanin binds microtubules using a multimeric microtubule-binding domain. *Plant Physiol. Biochem.*, **45**, 867–877.

43. Stöhr, H., Molday, L.L., Molday, R.S., Weber, B.H., Biedermann, B., Reichenbach, A. and Krämer, F. (2005) Membrane-associated guanylate kinase proteins MPP4 and MPP5 associate with Veli3 at distinct intercellular junctions of the neurosensory retina. *J. Comp. Neurol.*, **481**, 31–41.

44. MacKenzie, D., Arendt, A., Hargrave, P., McDowell, J.H. and Molday, R.S. (1984) Localization of binding sites for carboxyl terminal specific anti-rhodopsin monoclonal antibodies using synthetic peptides. *Biochemistry*, **23**, 6544–6549.

45. Maerker, T., van Wijk, E., Overlack, N., Kersten, F.F.J., McGee, J., Goldmann, T., Sehn, E., Roepman, R., Walsh, E.J., Kremer, H. and Wolfrum, U. (2008) A novel Usher protein network at the periciliary reloading point between molecular transport machineries in vertebrate photoreceptor cells. *Hum. Mol. Genet.*, **17**, 71–86.

46. Katoh, K., Kuma, K., Toh, H. and Miyata, T. (2005) MAFFT version 5: improvement in accuracy of multiple sequence alignment. *Nucleic Acids Res.*, **33**, 511–518.

47. Cole, C., Barber, J.D. and Barton, G.J. (2008) The Jpred 3 secondary structure prediction server. *Nucleic Acids Res.*, **36**, W197–201.